ACS OMEGA

http://pubs.acs.org/journal/acsodf

Article

Nitrogen-Doped TiO_2/Nitrogen-Containing Biochar Composite Catalyst as a Photocatalytic Material for the Decontamination of Aqueous Organic Pollutants

Zuhong Xiong, Hongyuan Chen, Lili Lu, Rui Shan,* Yuyuan Zhang, Haoran Yuan, and Yong Chen

Cite This: *ACS Omega* 2023, 8, 791−803

Read Online

ACCESS | Metrics & More | Article Recommendations | Supporting Information

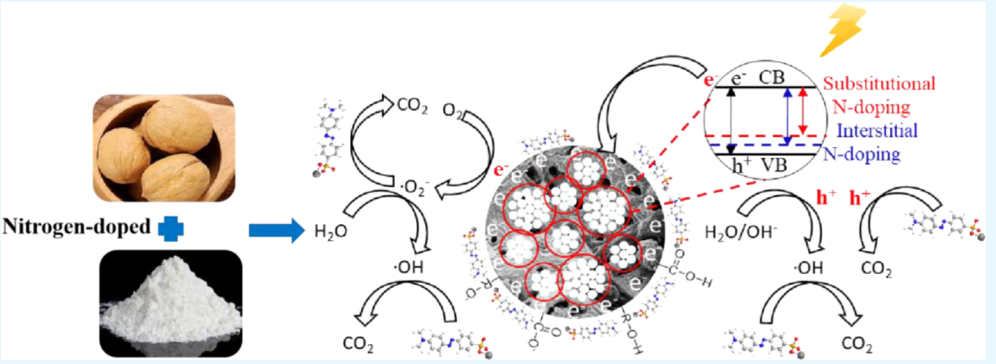

ABSTRACT: In this study, a waste walnut shell-derived biochar enriched with nitrogen (N-biochar) is mixed with nitrogen-doped TiO_2 (N-TiO_2) to fulfill an affordable composite material for the degradation of methyl orange (MO). Results showed that porous structure and oxygen-containing functional groups of biochar facilitate contact with MO during the reaction process. Meanwhile, doped nitrogen has a positive effect on improving the reaction activity due to the existence of a substituted state and a gap state in the catalyst. It was revealed that the N-TiO_2/N-biochar (NCNT0.2/1) exhibited better photocatalytic degradation efficiency (97.6%) and mineralization rate (85.4%) of MO than that of TiO_2, N-TiO_2, and TiO_2/N-biochar due to its stronger synergistic effect of N, TiO_2, and biochar, in accordance with its high charge separation by photoluminescence (PL) analysis. Trapping experiments showed that ·OH is the predominant active species during the decolorization and mineralization process of MO. After five repeated use, the loss of activity of the catalyst was negligible. In addition, the catalytic degradation process was consistent with the pseudo-first-order kinetic model with the rate constant of 4.02×10^{-2} min^{-1}.

1. INTRODUCTION

Photocatalytic technology becomes an emerging advanced oxidation technology that converts solar energy into chemical energy and decomposes pollutants, often used in air purification and wastewater treatment.[1−4] TiO_2 has low cost, good chemical stability, low toxicity, and excellent photoelectric performance.[5,6] Nevertheless, TiO_2 has a large band gap (E_g = 3.4 eV) and can only be activated by ultraviolet light, which indicates that the visible light utilization rate is low. At the same time, the charge recombination efficiency of TiO_2 is very high.[7] Therefore, TiO_2 is often modified to reduce its charge recombination efficiency.

The nonmetal-doped TiO_2 will form new impurity energy levels above the valence bond band, which reduces the band gap and promotes the red-shift of the absorption edge.[8−14] That means that the doped TiO_2 can obtain significant photocatalytic activity under visible-light irradiation. For instance, Chen et al.[15] found that the nitrogen-doped method could result in the enhancement of visible-light absorption and the generation of photoinduced surface oxygen vacancies. Giannakas et al.[16] prepared an N-TiO_2 catalyst with ammonium chloride as the nitrogen source and applied it to the reduction of Cr(VI). It showed that N-TiO_2 had a higher reduction ability than TiO_2, and the absorption of N-TiO_2 was enhanced at visible wavelength. Zhou et al.[17] prepared four different ratios of N-TiO_2/sepiolite photocatalysts and applied them to degrade lightfast orange G. The result indicated the activity of the four catalysts was superior to that of the TiO_2/sepiolite catalyst.

It is reported that the adsorbent on the surface of TiO_2 can significantly promote the photocatalytic process, such as

Received: September 22, 2022
Accepted: December 9, 2022
Published: December 23, 2022

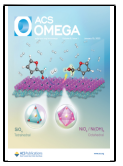

ACS Publications

© 2022 The Authors. Published by American Chemical Society

https://doi.org/10.1021/acsomega.2c06127
ACS Omega 2023, 8, 791−803

activated carbon,[18] carbon nanotubes,[19] and biochar.[20,21] Biochar, as an electron acceptor, can accelerate charge separation and transfer, thereby promoting the generation of active oxygen and improving the degradation performance of TiO_2.[22] Matos et al.[23] first prepared nitrogen-doped biochar as an adsorbent and then compounded it with TiO_2 to obtain a TiO_2/nitrogen-doped biochar catalyst. It was found that the nitrogen functional group in the biochar played an important role in the enhancement of reaction activity. Vahidzadeh et al.[24] prepared TiO_2/GO, N-TiO_2/GO, TiO_2/N-GO, and N-TiO_2/N-GO composite catalysts and then used them to degrade acetaldehyde. The results showed that N-TiO_2/N-GO catalysts had the highest activity compared with other catalysts due to the improvement of charge separation by their nitrogen site.

In our previous work,[25] we found that a proper amount of biochar was beneficial to improving the photocatalytic activity of TiO_2. For the TiO_2/biochar composite system, if nitrogen was simultaneously doped into the structure of TiO_2 and biochar, which might provide an opportunity to enhance charge separation and facilitate the generation of active oxygen. However, it was rarely studied in the photocatalytic process. For the above reasons, a series of nitrogen-doped TiO_2/nitrogen-containing biochar composite catalysts were prepared for the photodegradation of MO (as the model molecule of dye). The morphology, microstructure, and light absorption of the samples were systematically studied by various characterization methods, including scanning electron microscopy (SEM), X-ray diffraction (XRD), Fourier transform infrared spectroscopy (FT-IR), Raman spectra (Raman), ultraviolet−visible diffuse reflectance spectra (UV−vis DRS), and photoluminescence (PL). In addition, the photodegradation kinetics, mechanism, and reproducibility of the catalysts were discussed in detail.

2. MATERIALS AND METHODS

2.1. Materials. As a raw material for this research, the walnut shell was purchased in Guangzhou; tetrabutyl titanate (TBOT, 99.8%) and MO (96.0%) were purchased from Alfa Aesar China; and N_2 (99.9%) and NH_3 (99.99%) were purchased from Guangzhou Conghua Xinhe Co., Ltd.

2.2. Catalyst Preparation. Walnut shell was prepared through deionized water cleaning, followed by being dried in a blast drying oven at a temperature of 80 °C. After drying, the walnut shell was pulverized and passed through a sieve of 60 mesh to select particles with a diameter of less than 0.25 mm. The rice husk powder was screened and placed in a tube furnace and heated to 700 °C under the atmosphere of nitrogen (purity 99.99%) at a rate of 10 °C/min and thermostated for 2 h to obtain walnut shell biochar, which was named WB700. The prepared walnut shell biochar was heated to 500 °C in an NH_3 atmosphere for 1 h and calcined to obtain the nitrogen-doped biochar, which was named N-WB700.

TiO_2/biochar composites were prepared by direct hydrolysis combined with high-temperature calcination. Ten milliliters of tetrabutyl titanate was added dropwise into 100 mL of ultrapure water and stirred for 12 h. Then, a certain amount of biochar (biomass and titanium mass ratio of 0.2/1) was added and stirred for 12 h. The prepared suspension was dried for 24 h in an air dry oven at 80 °C. After drying and grinding, the sample was heated in a tube furnace to 500 °C for 1 h under the atmosphere of nitrogen. The obtained sample was named CT0.2/1.

The preparation procedure of the TiO_2/nitrogen-doped biochar composite material was similar to that of CT0.2/1. In detail, the nitrogen-doped TiO_2/nitrogen-doped biochar composite catalyst was prepared by simple heat treatment under an NH_3 atmosphere. Ten milliliters of tetrabutyl titanate was dispersed into 100 mL of ultrapure water dropwise. After being stirred for 12 h, a certain amount of biochar (the mass ratio of biochar and titanium was 0.1/1, 0.2/1, 0.5/1, 0.8/1, and 1/1, respectively) was added to the mixed solution and uninterruptedly stirred for 12 h. The suspension was dried in an air dry oven at 80 °C for 24 h. After drying and grinding, the sample was placed in a tube furnace and heated at a rate of 2 °C/min to 500 °C for 1 h under the atmosphere of NH_3. The calcined samples were nitrogen-doped composite catalysts, which were named NCNT0.1/1, NCNT0.2/1, NCNT0.5/1, NCNT0.8/1, and NCNT1/1, respectively. For comparison, a nitrogen-doped TiO_2 catalyst without the support of biochar was prepared and named N-TiO_2.

2.3. Catalyst Characterization. The crystal structure of the catalyst was measured by XRD spectra (PANALYTICAL Incorporated) under room temperature with the range of angle (10−80°). The surface chemistry of the catalyst was analyzed by FT-IR (TENSOR27) and Raman spectra (LabRAM HR800-LSS5). While the surface morphology of catalysts was studied by SEM (Hitachi S-4800), and the surface element distribution of the catalyst was observed by an energy spectrometer matched with a scanning electron microscope. The chemical bonding state in the catalyst was analyzed by X-ray photoelectron spectroscopy (XPS, Thermo Scientific ESCALAB250Xi) measured by a spectrometer. The UV−vis DRS of the catalyst was measured at room temperature using a Shimadzu UV 3600 spectrophotometer within the wavelength of 200−700 nm with $BaSO_4$ as a reflectance standard. The PL was measured by LabRAM HR800-LSS5 with an excitation wavelength of 325 nm.

2.4. Photocatalytic Degradation of MO. The photocatalytic degradation experiment of methyl orange was carried out by a multisite photocatalytic reactor with a circular reaction platform as well as a quartz cold trap. A long arc mercury lamp (500 W) was used as an ultraviolet light source with a constant voltage and current, and the dominant wavelength was 360 nm. During the experiment, 10 mg of the catalyst was added into 40 mL of the MO solution (20 mg/L), followed by stirring for 1 h in the dark to achieve adsorption equilibrium, and then the mercury lamp was turned on while stirring. To remove the catalyst, an appropriate amount of the solution was taken out from the test tube and filtered with a filter (PES, JINTENG) of 0.22 μm for subsequent analysis. The photocatalytic activity of the catalyst was assessed by the decolorization and mineralization rate of MO; the absorbance of MO was measured by a spectrophotometer (Lambda 750, Perkinelmer) with the maximum absorption wavelength of 464 nm to determine the concentration. The mineralization rate is determined by the total organic carbon (TOC) obtained from the total organic carbon analyzer (Vario TOC, Elementar).

The decolorization rate is calculated by the following formula

https://doi.org/10.1021/acsomega.2c06127
ACS Omega 2023, 8, 791−803

decolorization effiency (%)

$$= 100 \times ([MO]_0 - [MO]_t)/[MO]_0 \quad (1)$$

In eq 1, $[MO]_0$ represents the MO initial concentration (mg/L);

[MO] represents the real-time concentration of *t*-methyl orange (mg/L).

The mineralization rate is calculated with the following formula

mineralization efficiency (%)

$$= 100 \times ([TOC]_0 - [TOC]_t)/[TOC]_0 \quad (2)$$

In eq 2, $[TOC]_0$ represents the initial total organic carbon (mg/L) of MO;

$[TOC]_t$ represents MO in real-time total organic carbon (mg/L).

2.5. Ultraperformance Liquid Chromatography-Quadrupole-Time-of-Flight Mass Spectrometry (UPLC-QTOF). Intermediates during the degradation were analyzed by an ultrahigh-resolution quadrupole time-of-flight mass spectrometer (Agilent 1290-6540, America). During the experiment, a C18 column (50 mm × 2.1 mm, particle size 1.9 μm) and a mobile phase consisting of 10 mM ammonium acetate (A) and acetonitrile (B) were used at a flow rate of 0.2 mL/min.

2.6. Catalyst Reuse Experiment. NCNT0.2/1 with the best catalytic performance was selected for reuse experiments. After the degradation experiment, the catalyst was washed with deionized water and dried for 24 h at 80 °C. The dried catalyst was continued to be used for the next experiment. The experimental data was acquired by three replicates at the same condition and expressed as mean value ± SD.

3. RESULTS AND DISCUSSION

3.1. Characterizations of the TiO_2/Nitrogen-Doped Biochar Composite Catalyst. As shown in Figure 1a,b, both WB700 and N-WB700 prepared by pyrolysis of charcoal-shelled charcoal at 700 °C exhibited a porous structure and high porosity, which is beneficial for the adsorption of organic matter. The morphologies of TiO_2, N-TiO_2, and NCNT0.2/1 are shown in Figure 1c,f–h. It was clear that TiO_2 particles with a size of several nanometers were agglomerated into large particles of several tens of micrometers. N-TiO_2 obtained by calcination under an NH_3 atmosphere is shown in Figure 1d, and its morphology was similar to that of TiO_2. As shown in Figure 1e, compared with TiO_2, the TiO_2 particles in NCNT0.2/1 are more uniformly distributed on the surface of biochar, resulting in the improvement of the agglomeration phenomenon of the TiO_2 particles. At the same time, the porous structure of biochar was beneficial to the adsorption of organic matter, enhancing the interaction between the organic matter and catalyst. The heterostructure of TiO_2 and biochar facilitated the photogenerated electrons transfer from TiO_2 to biochar, which enhances the photocatalytic performance of TiO_2.

Figure 2 shows the SEM-EDS mapping of N-WB700, N-TiO_2, and NCNT0.2/1, suggesting the presence of nitrogen in the three catalysts. The EDS mapping of N-WB700 showed that the N site was doped into biochar by pyrolysis of the walnut shell under an NH_3 atmosphere. Also, a similar conclusion was observed by N-TiO_2 based on the EDS mapping image. As for NCNT0.2/1, it was clear that the nitrogen element in the samples was present in both biochar and TiO_2.

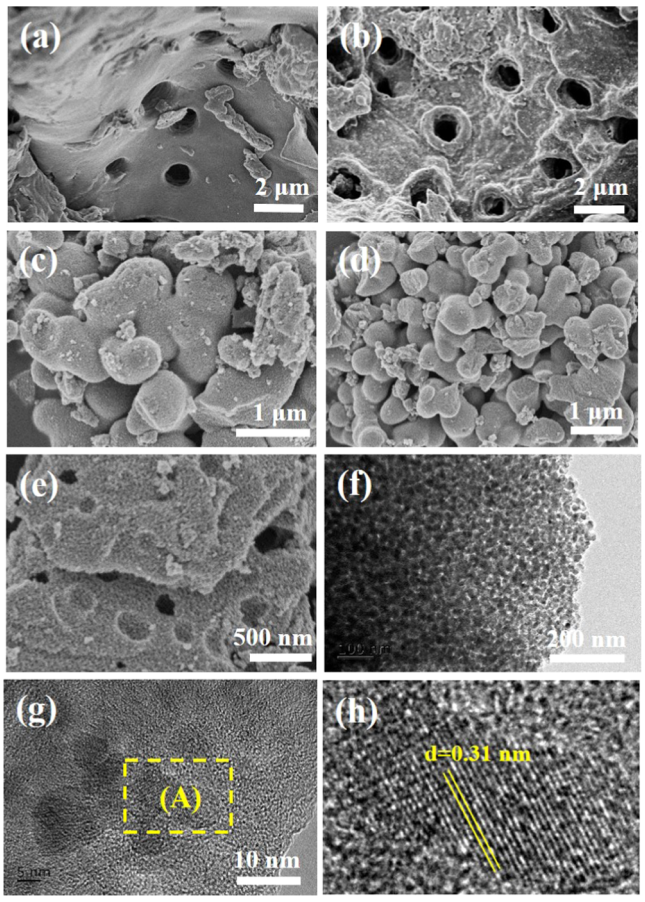

Figure 1. SEM images of (a) WB700, (b) N-WB700, (c) TiO_2, (d) N-TiO_2, and (e) NCNT0.2/1. (f) TEM image of TiO_2, (g) HRTEM image of TiO_2, and (h) magnified view of spot A marked in (g).

Figure 3 demonstrated the XRD patterns of TiO_2, N-TiO_2, CT0.2/1, NCT0.2/1, NCNT0.2/1, and NCNT0.8/1. The two characteristic diffraction peaks at 2θ = 25.3 and 37.8° corresponded to the (101) and (004) crystal planes of anatase TiO_2.[26] In comparison to the brookite crystal and the rutile crystal, anatase TiO_2 had high catalytic activity, which is mainly due to its larger oxygen vacancies, lower dielectric constant, and higher electron mobility.[27] As shown in Figure 3, the diffraction peak shape of TiO_2 corresponded to the anatase TiO_2 characteristic peak. However, the characteristic peak of nitrogen did not appear in N-TiO_2, which was attributed to small amount of nitrogen, and the approximate radius between N and Ti results in the weak intensity of its characteristic peaks. For CT0.2/1, NCT0.2/1, NCNT0.2/1, and NCNT0.8/1, the peak of anatase showed that the higher intensity and peak shape were intact, suggesting that the presence of biochar did not cause a change in the crystal form of TiO_2. There was no characteristic peak of biochar in the spectrum, which was mainly because the characteristic peak intensity of biochar was low and close to the characteristic peak of anatase crystal. For the NCT0.2/1, NCNT0.2/1, and NCNT0.8/1 composite catalysts, no characteristic peaks of nitrogen were observed in the XRD spectrum, mainly due to the small amount of nitrogen in the sample. In short, we successfully synthesized the composite catalysts with the anatase crystal form.

https://doi.org/10.1021/acsomega.2c06127
ACS Omega 2023, 8, 791−803

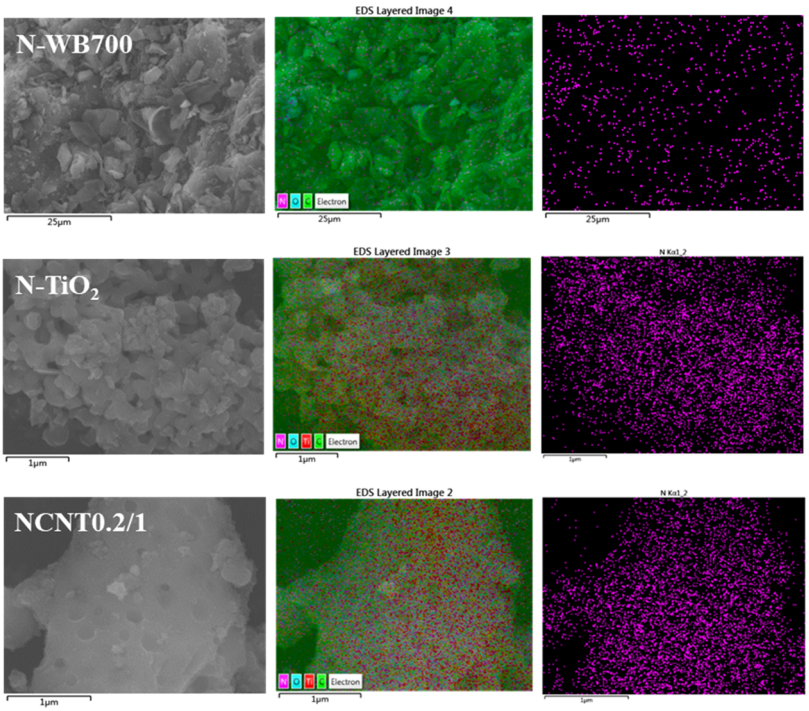

Figure 2. SEM-energy-dispersive spectra (SEM-EDS) mapping images of catalysts.

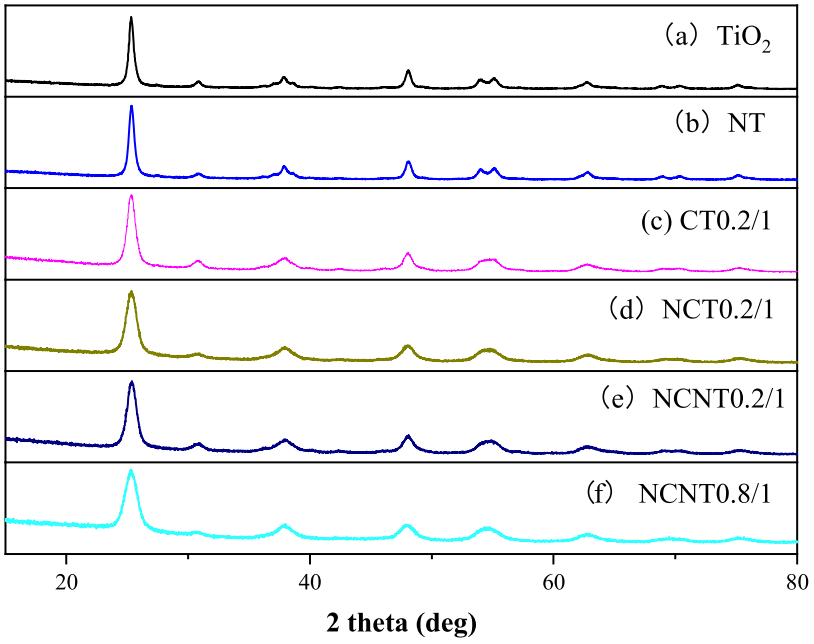

Figure 3. XRD patterns of (a) TiO_2, (b) N-TiO_2, (c) CT0.2/1, (d) NCT0.2/1, (e) NCNT0.2/1, and (f) NCNT0.8/1.

Figure 4 exhibits the Raman spectrum of the prepared samples. As for WB700, N-WB700, CT0.2/1, NCT0.2/1, NCNT0.2/1, and NCNT0.8/1, the D peak and G peak were located at 1348.1 and 1590.1 cm^{-1}, which was assigned to a carbon defect-induced Raman peak and an ordered graphite structure peak, respectively. Therefore, the presence of biochar can be confirmed for the composite catalyst. In general, for TiO_2 with the anatase phase, the peaks at 142.0, 396.3, 513.1, and 637.2 cm^{-1} can be clearly observed, corresponding to the Raman vibration modes of E_g, B_{1g}, B_{1g} + A_{1g}, and weak E_g, respectively.[28] These peaks of anatase TiO_2 were also observed in TiO_2, N-TiO_2, CT0.2/1, NCT0.2/1, NCNT0.2/1, and NCNT0.8/1. The degree of graphitization (IG/ID) of WB700 and N-WB700 was 0.84 and 0.90, respectively, while the IG/ID ratios of CT0.2/1, NCT0.2/1, NCNT0.2/1, and NCNT0.8/1 composite catalysts were decreased to 0.78, 0.77, 0.79, and 0.81, respectively. This suggested negligible disadvantages of the combination between TiO_2 and biochar.

The XPS spectra of CT0.2/1, N-WB700, N-TiO_2, and NCNT0.2/1 are illustrated in Figure 5. All binding energy values were calibrated by the reference carbon at 284.8 eV. The peaks of C 1s, O 1s, and Ti 2p of the CT0.2/1 catalyst were clearly observed in the spectrum, suggesting the presence of C, O, and Ti elements; the peaks of C 1s, Ti 2p, O 1s, and N

https://doi.org/10.1021/acsomega.2c06127
ACS Omega 2023, 8, 791−803

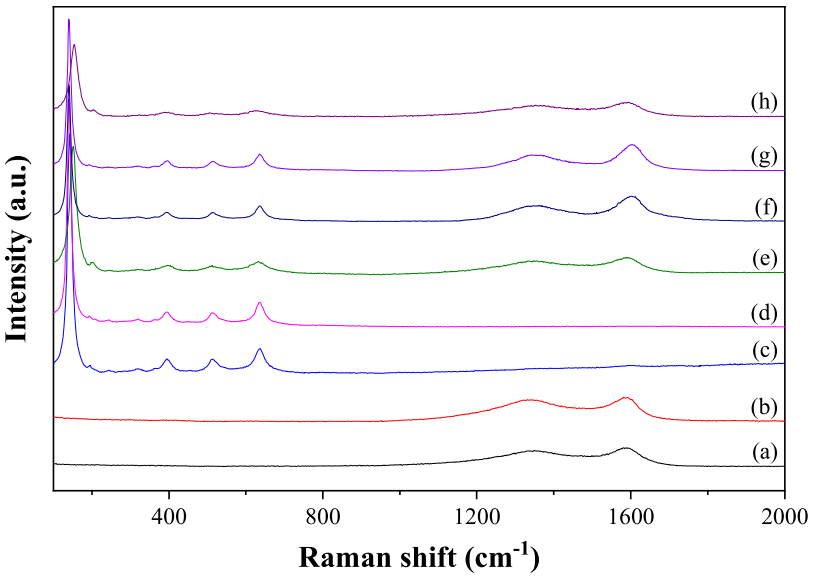

Figure 4. Raman spectra of (a) WB700, (b) N-WB700, (c) TiO_2, (d) N-TiO_2, (e) CT0.2/1, (f) NCT0.2/1, (g) NCNT0.2/1, (h) NCNT0.8/1.

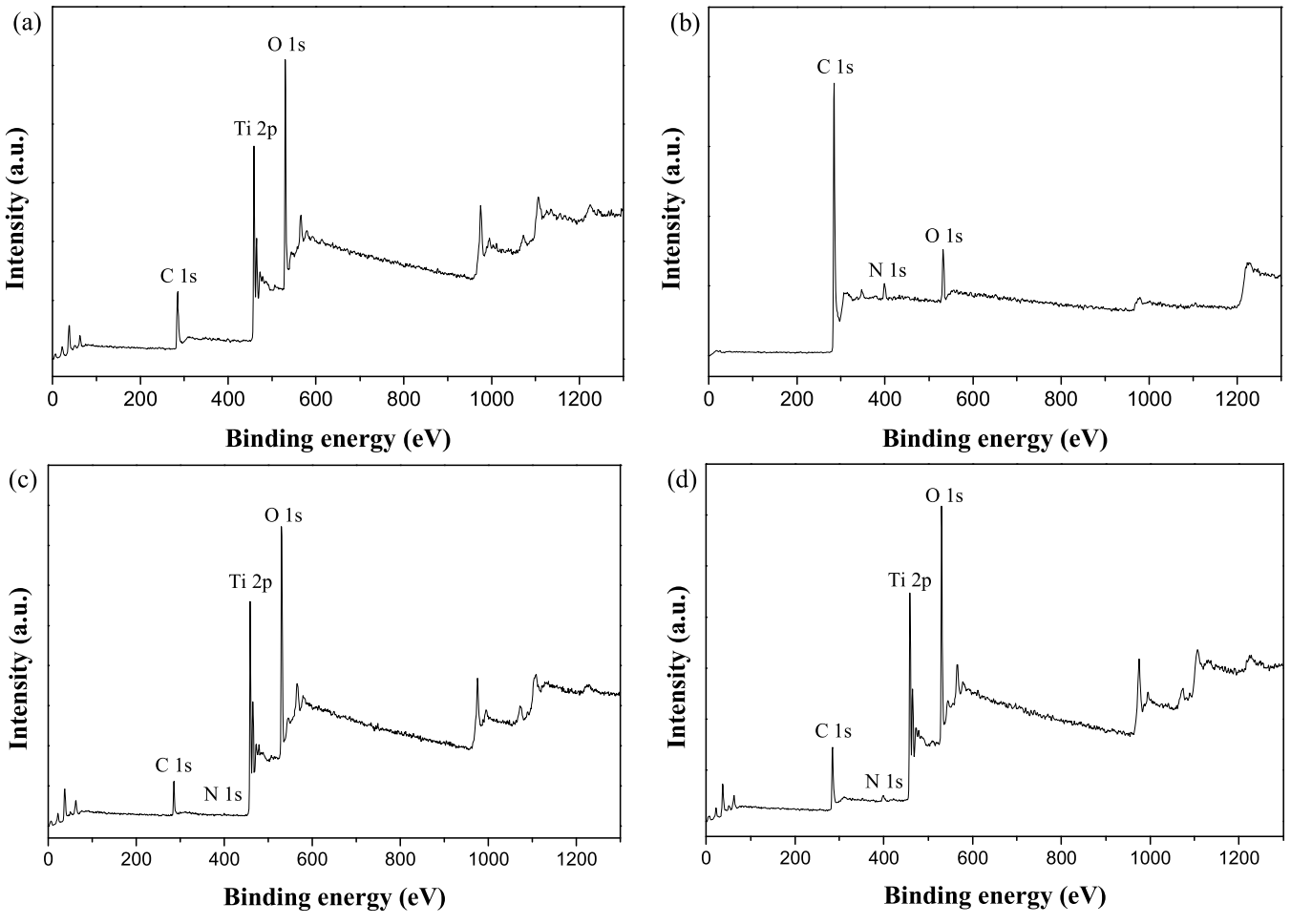

Figure 5. XPS wide scan spectra of (a) CT0.2/1, (b) N-WB700, (c) N-TiO_2, and (d) NCNT0.2/1.

1s were observed in the spectra of N-WB700, N-TiO_2, and NCNT0.2/1, indicating that the catalyst was composed of C, Ti, O, and N elements.

Figure 6 shows the XPS spectra of N 1s in N-WB700, N-TiO_2, and CNT0.2/1. As shown in Figure 6a, the weak intensity of N 1s in the CT0.2/1 catalyst was observed, indicating that there was basically no nitrogen on the surface of the catalyst. As shown in Figure 6b, the N 1s of the N-WB700 sample could be deconvoluted into three peaks, corresponding to pyridinium nitrogen at 398.3 eV, pyrrole nitrogen at 399.6 eV, graphite nitrogen at 400.7 eV, and NO_x at 402.0 eV.[11] The N 1s peak of N-TiO_2 was fitted to four peaks located at 397.2,

https://doi.org/10.1021/acsomega.2c06127
ACS Omega 2023, 8, 791−803

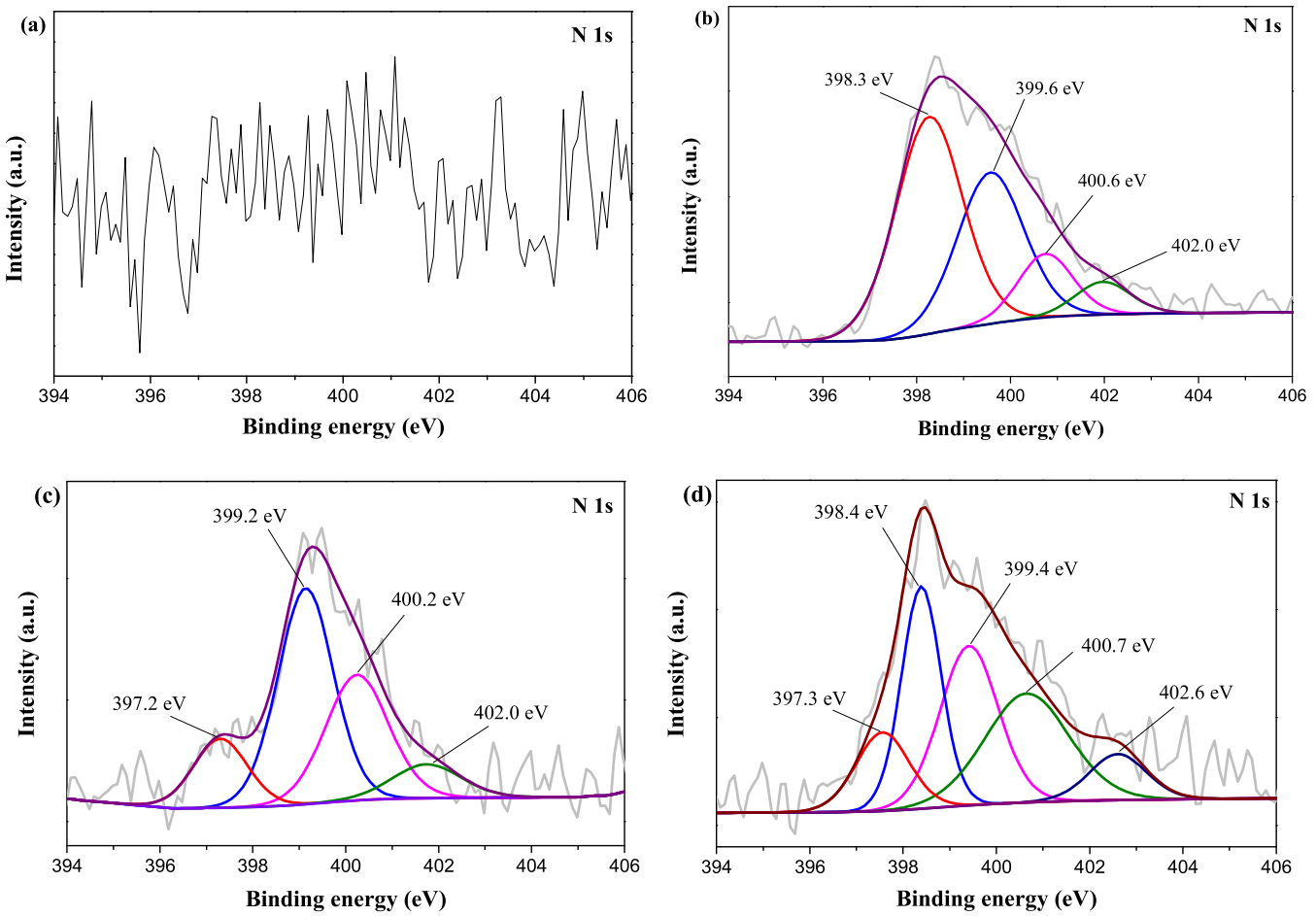

Figure 6. XPS spectra of N 1s in (a) CT0.2/1, (b) N-WB700, (c) N-TiO_2, and (d) NCNT0.2/1.

399.2, 400.2, and 402.0 eV. The N 1s peak of N-TiO_2 was generally attributed to the Ti−N bond based on the previous literature.[29] In this work, the peak of 397.3 eV was attributed to the Ti−N bond from substituted N dopant, while the peaks of 399.2 and 400.2 eV corresponded to interstitial N dopants, typically, as stated by Fujishima et al.[30] The peak of 402.0 eV was attributed to the presence of chemically adsorbed NO_x. Generally, when nitrogen entered the TiO_2 lattice in the form of substitution or gap state, new impurity levels were formed between valence and conduction bands, which would promote small band gap and improve the photocatalytic activity of TiO_2.[31,32] The N 1s spectrum of NCNT0.2/1 is shown in Figure 6d and deconvoluted into five peaks located at 397.3, 398.4, 399.4, 400.7 and 402.6 eV. Peaks at 397.3 and 402. 6 eV were assigned to the substituted nitrogen and NO_x, respectively. The peaks of 398.4, 399.4, and 400.7 eV were derived from interstitial nitrogen, indicating that the nitrogen atom had entered the interstitial site. For NCNT0.2/1, nitrogen entered the TiO_2 lattice in the form of substituted and gap states, which decrease its band gap and improve its visible-light response.

As shown in Figure 7, all of the catalysts exhibited an absorption peak below 380 nm, indicating that samples had strong ultraviolet light absorption. Due to the presence of nitrogen and biochar, the light absorption of the composite catalyst in the visible-light band was enhanced. With the increase of the biochar content, the absorbance in the visible-light region increased gradually.

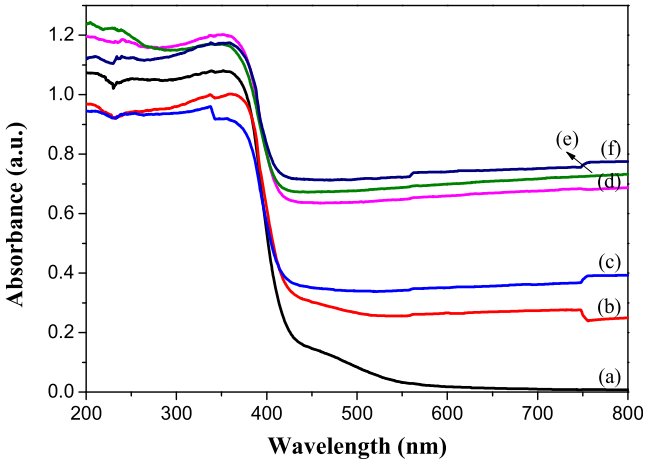

Figure 7. UV−vis DRS spectra of (a) N-TiO_2, (b) NCNT0.1/1, (c) NCNT0.2/1, (d) NCNT0.5/1, (e) NCNT0.8/1, and (f) NCNT1/1.

The band gap of the catalyst was estimated by the Kubelka−Munk equation and the value was given by the baseline method provided by Makuła.[33] As shown in Figure 8, the E_g values of N-TiO_2, NCNT0.1/1, NCNT0.2/1, NCNT0.5/1, NCNT0.8/1, and NCNT1/1 catalysts were 3.01, 3.00, 3.01, 3.03, 3.03, and 3.05 eV. The decrease in the band gap of the nitrogen-doped catalyst was attributed to the fact that the nitrogen element in the TiO_2 promotes the generation of a substituted or gap state.

https://doi.org/10.1021/acsomega.2c06127
ACS Omega 2023, 8, 791−803

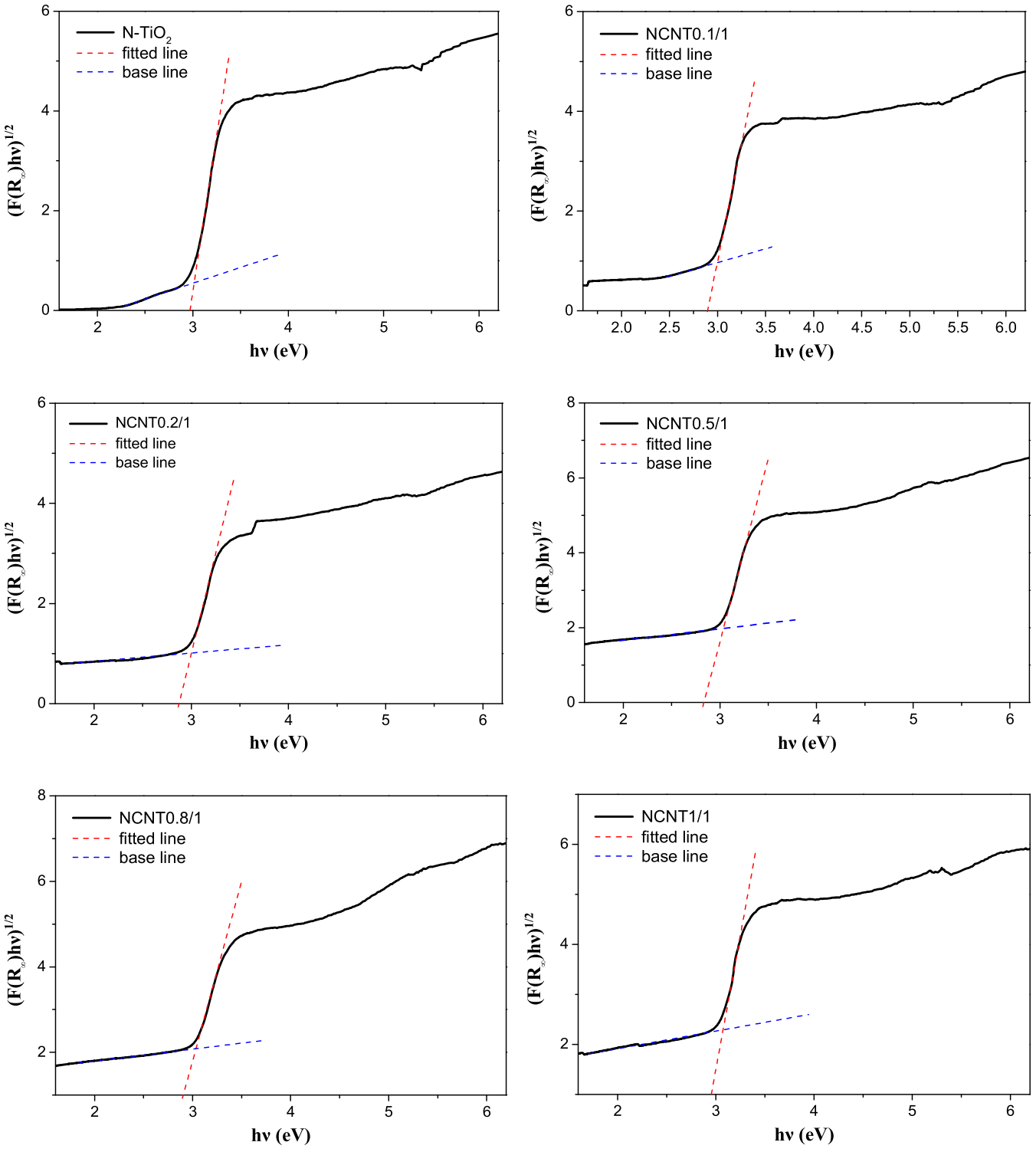

Figure 8. Band gap of different catalysts.

PL spectra were commonly used to study the efficiency of electron−hole pair separation. In general, the greater intensity of PL spectra is closely associated with the higher recombination rate of photogenerated charge and the lower photocatalytic activity.[34] As shown in Figure 9, with the excitation wavelength of 325 nm, similar PL spectra of these samples were observed (the strongest peak at about 390 nm). NCNT0.2/1 had the lowest intensity of PL spectra, indicating its highest efficiency of charge separation and photocatalytic activity.

3.2. Photocatalytic Degradation of MO. As shown in Figure 10, the decolorization efficiencies of CT0.1/1, CT0.2/1, CT0.5/1, CT0.8/1, and CT1/1 for MO were 65.7, 76.4, 62.6, 46.6, and 42.9%, respectively. However, the decolorization efficiencies of the N-doped catalysts were 89.3, 97.6, 90.4, 74.2, and 66.7%, which were an increase of 35.9, 27.8, 44.4, 58.8, and 55.4%, respectively. When the TiO_2/biochar composite

https://doi.org/10.1021/acsomega.2c06127
ACS Omega 2023, 8, 791−803

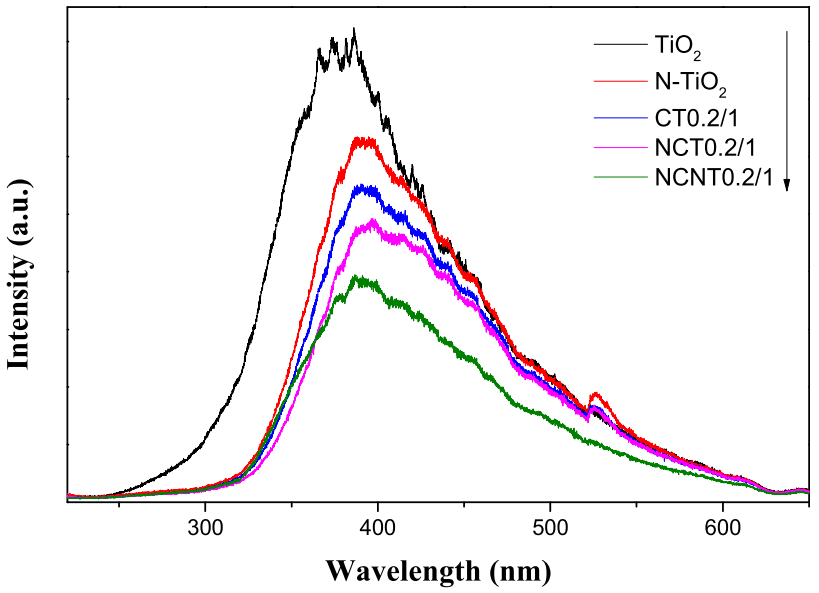

Figure 9. PL spectra of different catalysts.

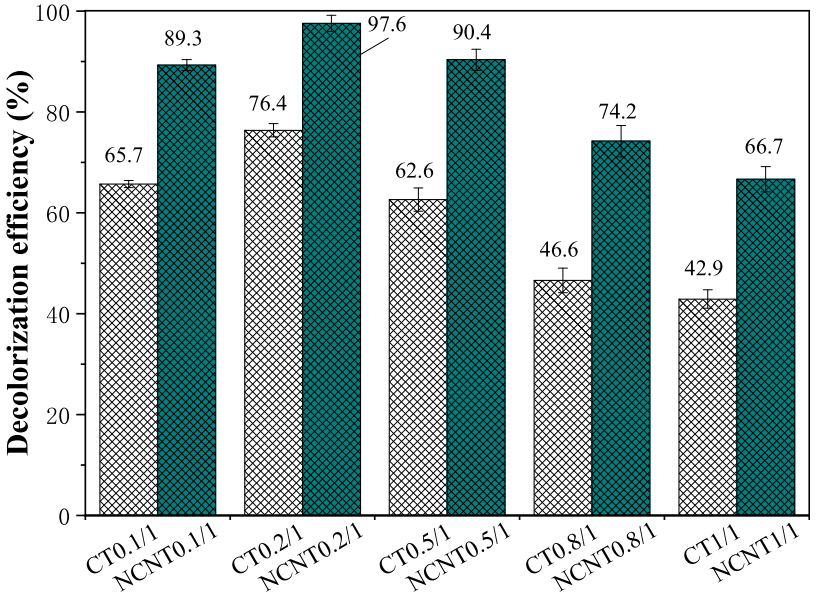

Figure 10. Degradation efficiency of MO with different catalysts. Conditions: $[MO]_0$, 20 mg/L; MO solution, 40 mL; catalyst amount, 10 mg; and UV irradiation time, 90 min.

catalyst was mixed with nitrogen, the degradation rate of MO was improved because of the synergistic effect of nitrogen-doped TiO_2 and nitrogen-doped biochar. Also, it can be observed that NCNT0.2/1 had the highest photocatalytic activity, which was mainly due to the optimal value of biochar content. Because excessive biochar had a filtering effect on light, it would hinder light from reaching the catalyst surface and suppress the photon absorption on the surface of TiO_2, thus reducing the performance of the catalyst.

To explore the mechanism of the catalytic activity of nitrogen-doped catalyst/nitrogen-doped biochar composite catalyst, a series of catalysts were prepared for control experiments. Figure 11 shows the results of a series of experiments for the degradation of MO. During the photolysis experiment of MO, the decolorization and mineralization efficiencies were 2.1 and 1.8%, indicating that the MO molecules were hard to self-degrade under only visible light. When TiO_2 was present, the decolorization rate and mineralization rate were 52.6 and 34.2%. When N-TiO_2 was presented, the decolorization rate and mineralization rate were 78.4 and 60.6%. An increase in activity may be due to the formation of a new nitrogen impurity level above the valence band from the interstitial nitrogen or substituted nitrogen in the structure of TiO_2, which resulted in a decrease in the semiconductor band gap and an increase in the absorption in the visible-light region.[35] In comparison with pure TiO_2, the decolorization and mineralization rate of MO on CT0.2/1 increased by 45.2 and 64.4%, respectively. The increased degradation rate was mainly attributed to the fact that biochar promoted photogenerated electron separation of TiO_2 and inhibited its electron−hole recombination. The degradation rate of MO by NCT0.2/1 was higher than that of CT0.2/1,

https://doi.org/10.1021/acsomega.2c06127
ACS Omega 2023, 8, 791−803

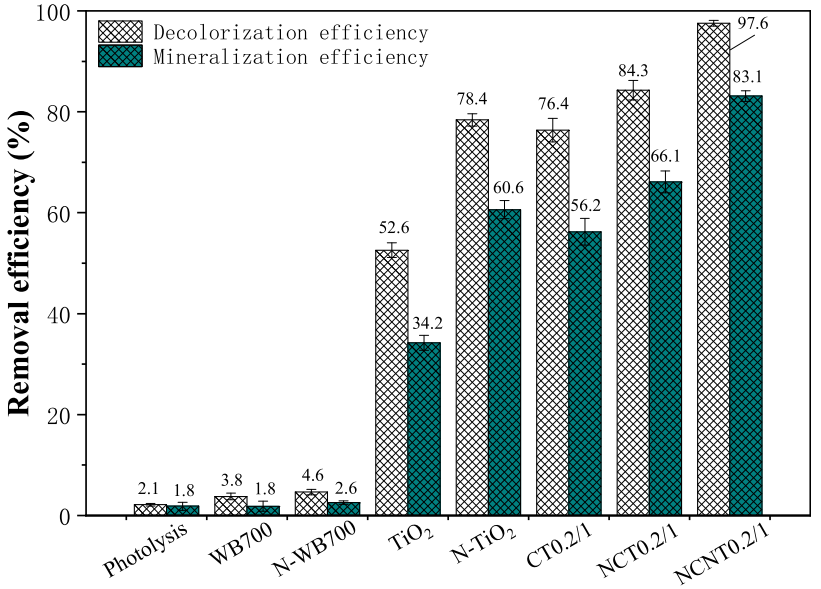

Figure 11. Degradation efficiency of MO with different samples. Conditions: $[MO]_0$, 20 mg/L; MO solution, 40 mL; catalyst amount, 10 mg; and UV irradiation time, 90 min.

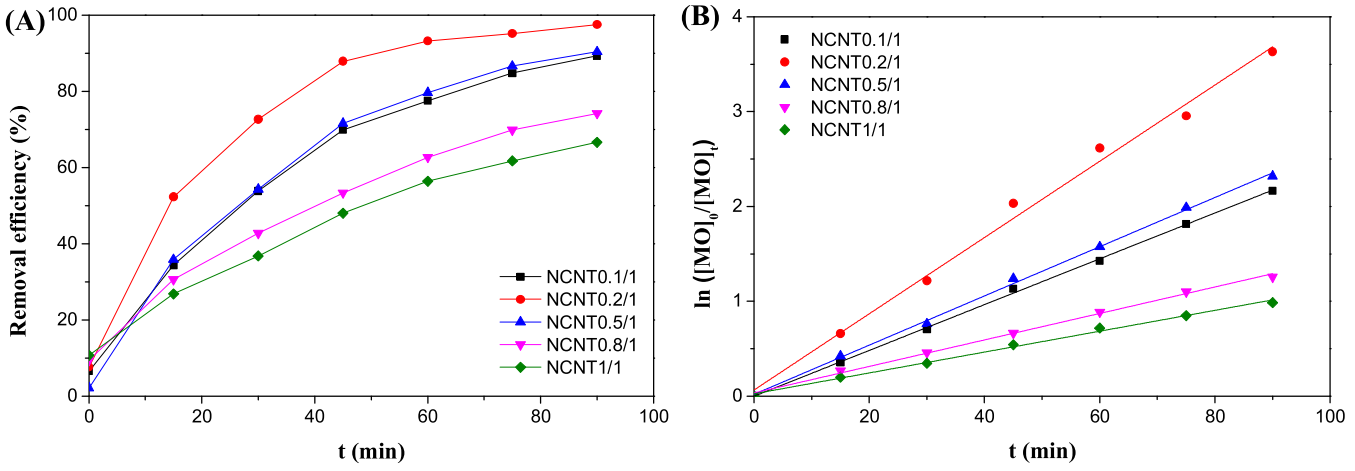

Figure 12. (A) Photocatalytic degradation of MO with different samples. (B) Photocatalytic degradation kinetics of MO. Conditions: $[MO]_0$, 20 mg/L; MO solution, 40 mL; catalyst amount, 10 mg; and UV irradiation time, 90 min.

and the reason may be that the presence of pyridinium nitrogen, pyrrole nitrogen, and graphite nitrogen in biochar improves the electron transfer. A similar conclusion has also been reported in the literature, and it has been shown that nitrogen-doped biochar can separate photogenerated charge carriers more efficiently than biochar.[36] NCNT0.2/1 had the highest degradation efficiency for methyl orange, and its decolorization rate and degradation rate reached 97.6 and 83.1%, respectively. Also, the electron-transfer efficiency of biochar was improved after adding nitrogen, which promoted the photoelectron transfer of N-TiO_2. Therefore, NCNT0.2/1 had the best performance, indicating that the synergistic effect of nitrogen-doped TiO_2 and nitrogen-doped biochar was beneficial to the improvement of catalyst activity.

3.3. Degradation Kinetics of Methyl Orange. Figure 12a shows the time curves of methyl orange for NCNT0.1/1, NCNT0.2/1, NCNT0.5/1, NCNT0.8/1, and NCNT1/1 composite catalysts. As illustrated in Figure 12b, the pseudo-first-order kinetic (PFOK) model is fitted well with most of the experimental data. The kinetic parameters determined by the (PFOK) model are listed in Table S1. The photocatalytic degradation was consistent with the first-order kinetics when all R^2 values were greater than 0.99. The catalyst NCNT0.2/1 had the largest degradation rate of 4.0×10^{-2} min^{-1}, and its degradation rate was obtained through theoretical analysis to provide guidance for practical application.

3.4. Catalyst Reproducibility. The stability and reproducibility of the catalyst are important for industrial applications. In this work, NCNT0.2/1 was selected for five repeated-use experiments due to its highest photocatalytic activity. As shown in Figure 13, after five cycles, NCNT0.2/1 maintains relatively high activity in the removal of MO, and the decolorization and mineralization rates reached 92.7 and 75.7%, respectively. The slightly decreased degradation efficiency was mainly because of the loss of catalysts. The results showed that NCNT0.2/1 exhibited desirable stability and reproducibility.

3.5. Degradation Mechanism Analysis. As shown in Figures S1 and S2 (in the Supporting Information), there was a strong peak at a retention time (RT) of 4.5 min, related to the MO molecule with m/z at 304. The peaks of RT 7.8, RT 10.0,

https://doi.org/10.1021/acsomega.2c06127
ACS Omega 2023, 8, 791−803

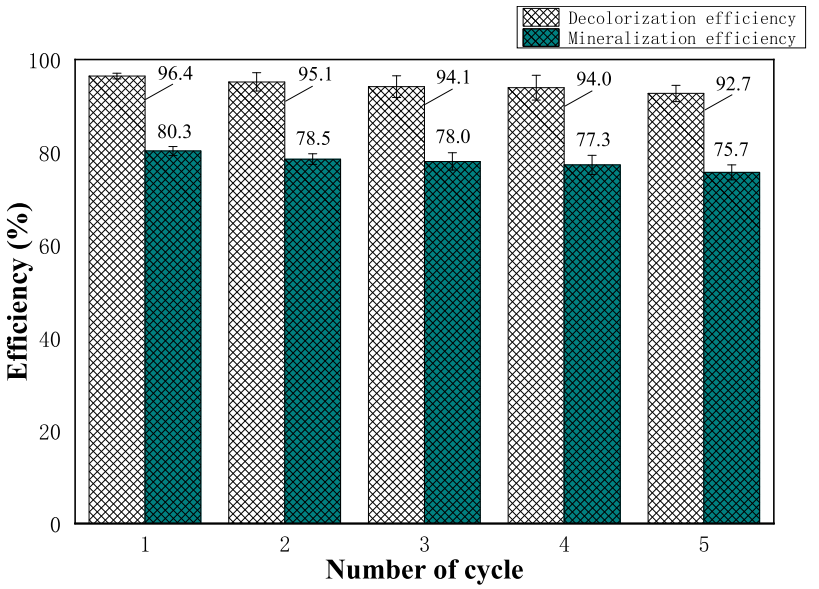

Figure 13. Reproducibility of the NCNT0.2/1 catalyst. Conditions: $[MO]_0$, 20 mg/L; MO solution, 40 mL; catalyst amount, 10 mg; and UV irradiation time, 90 min.

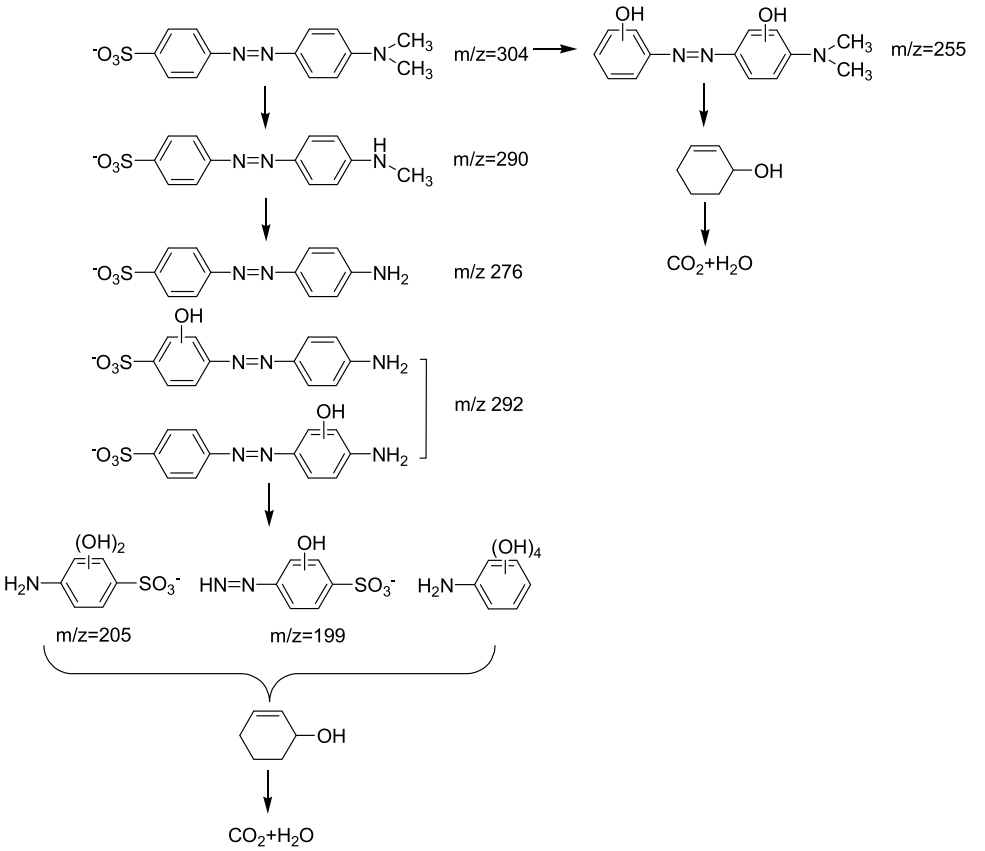

Figure 14. Proposed pathway for the photocatalytic degradation of MO.

RT 12.2, and RT 15.3 min were attributed to the intermediates produced by the self-degradation of MO. After irradiation by UV light for 40 min, the peak intensity at RT for 4.5 min decreased sharply due to the rapid decolorization of MO. Meanwhile, new peaks appeared at RT at 0.9, 1.5, 3.1, 3.2, and 3.8 min. The peak at 0.9 min (m/z 290) was related to the negative ion from a certain N−C bond cleavage of the dimethylamino group and a proton-substituted methyl group.[15] The peak at 3.1 min (m/z 276) corresponded to the cleavage of two N−C bonds of the dimethylamino group.[37] Also, the peak at 3.2 min was related to the monohydroxylation product of the MO molecule. The peak at 12.2 min (m/z 255) belonged to the dihydroxylated product of the MO molecule. The azo bond is then destroyed to form certain kinds of intermediates, like m/z 205, m/z 199, and m/z 157, which are attacked by reactive oxygen species and ultimately converted to

https://doi.org/10.1021/acsomega.2c06127
ACS Omega 2023, 8, 791−803

inorganic matter.[38] After irradiating for 90 min, it was found that the peak at 4.5 min disappeared, which meant the complete discoloration of MO. Also, three weak peaks at 10.0, 12.2, and 15.3 min indicate the presence of undegraded organic intermediates after decolorization. The enhanced peak at 0.9 min indicates the intermediate conversion of other complexes. Thus, Figure 14 presents the intermediate structure as well as the degradation pathway of MO.

For the photocatalytic reaction, hydroxyl radicals (·OH), superoxide anion radicals ($O_2\cdot^-$), and holes (h^+) are common active matters and probably participated in the degradation of organic matters. Active species trapping experiments were carried out using TEOA, IPA, and BQ as h^+, $O_2\cdot^-$, and ·OH trapping agents, respectively. As presented in Figure 15, after

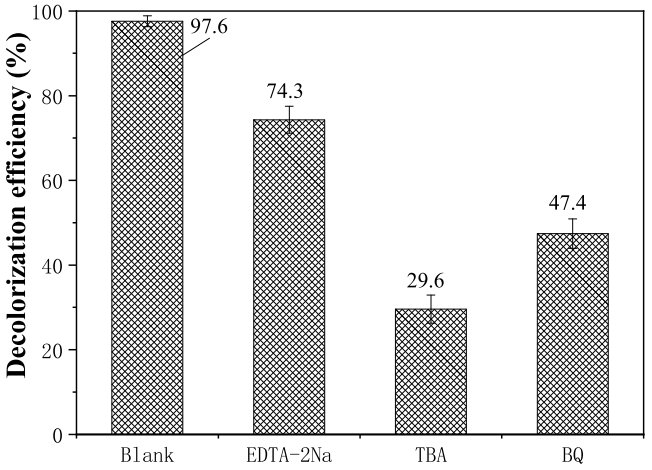

Figure 15. Photocatalytic oxidation of MO over the NCNT0.2/1 catalyst alone and with the addition of EDTA-2Na, TBA, and BQ.

the addition of TEOA, IPA, and BQ, the decolorization efficiency of MO decreased to 74.3, 29.6, and 47.4%, respectively. It can be concluded that the three active substances could possibly participate in the oxidation process, among which, ·OH plays a dominating role.

The possible degradation mechanism of MO by NCNT0.2/1 is shown in Figure 16. The well-developed pore structure and various oxygen-containing functional groups of biochar on NCNT0.2/1 provide more sites for the adsorption of organic pollutants. When irradiated by UV light, electrons of the N-TiO_2 were stimulated and migrated to the conduction band, while h^+ could leave in the valence band. Simultaneously, substitution nitrogen and interstitial nitrogen in the structure of NCNT0.2/1 could improve the utilization efficiency of visible light. On the other hand, this nitrogen could also promote the photogenerated electron transfer from TiO_2 to biochar, which enhances charge separation efficiency. The photogenerated electrons on the surface of biochar may react with O molecules to produce $O_2\cdot^-$ and further react with H_2O molecules to generate ·OH. In addition, h^+ are also trapped by H_2O molecules, producing ·OH. In the photocatalytic process, MO molecules could easily react with these active species (h^+, $O_2\cdot^-$, and ·OH) and finally mineralized into CO_2.

4. CONCLUSIONS

A series of nitrogen-doped TiO_2/nitrogen-doped biochar catalysts were prepared for the photodegradation of MO in an aqueous solution. In the photocatalytic control experiment, the removal efficiency followed the trend of NCNT0.2/1 > NCT0.2/1 > N-TiO_2 > CT0.2/1 > TiO_2, and NCNT0.2/1 showed the highest catalytic activity, with the decolorization rate and mineralization rate of 92.7 and 75.7%, respectively. By characterization analysis, it was found that the synergistic effect between nitrogen-doped TiO_2 and nitrogen-doped biochar improved the activity of catalysts. Furthermore, NCNT0.2/1 still showed relatively high degradation activity for MO after five repeated use. This NCNT0.2/1 catalyst with desirable activity and reproducibility for the treatment of environmental pollutants brings benefits to the disposal of discarded walnut shells.

■ ASSOCIATED CONTENT

Supporting Information

The Supporting Information is available free of charge at https://pubs.acs.org/doi/10.1021/acsomega.2c06127.

Parameters of the degradation kinetics of MO, chromatograms monitored in full scan MS, MS spectrum, and UV absorption spectra (PDF)

■ AUTHOR INFORMATION

Corresponding Author

Rui Shan − *Guangzhou Institute of Energy Conversion, Chinese Academy of Sciences, Guangzhou 510640, China;*

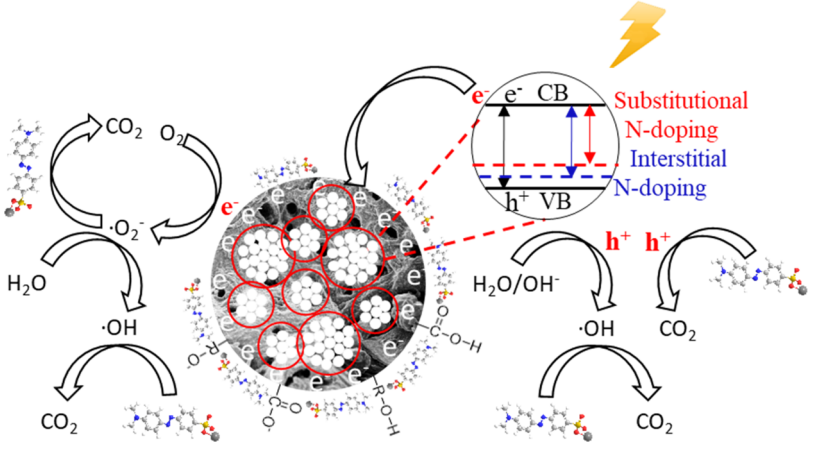

Figure 16. Schematic illustration of the degradation of MO over the as-prepared catalyst.

https://doi.org/10.1021/acsomega.2c06127
ACS Omega 2023, 8, 791−803

CAS Key Laboratory of Renewable Energy, Guangdong Provincial Key Laboratory of New and Renewable Energy Research and Development, Guangzhou 510640, China; orcid.org/0000-0002-6181-0061; Email: shanrui@ms.giec.ac.cn

Authors

Zuhong Xiong − *Guangzhou Institute of Energy Conversion, Chinese Academy of Sciences, Guangzhou 510640, China; CAS Key Laboratory of Renewable Energy, Guangdong Provincial Key Laboratory of New and Renewable Energy Research and Development, Guangzhou 510640, China*

Hongyuan Chen − *Guangzhou Institute of Energy Conversion, Chinese Academy of Sciences, Guangzhou 510640, China; CAS Key Laboratory of Renewable Energy, Guangdong Provincial Key Laboratory of New and Renewable Energy Research and Development, Guangzhou 510640, China; School of Engineering Science, University of Science and Technology of China, Hefei 230027 Anhui, China*

Lili Lu − *Guangzhou Institute of Energy Conversion, Chinese Academy of Sciences, Guangzhou 510640, China; CAS Key Laboratory of Renewable Energy, Guangdong Provincial Key Laboratory of New and Renewable Energy Research and Development, Guangzhou 510640, China*

Yuyuan Zhang − *School of Materials Science and Hydrogen Energy, Foshan University, Foshan 528000 Guangdong, China*

Haoran Yuan − *Guangzhou Institute of Energy Conversion, Chinese Academy of Sciences, Guangzhou 510640, China; CAS Key Laboratory of Renewable Energy, Guangdong Provincial Key Laboratory of New and Renewable Energy Research and Development, Guangzhou 510640, China;* orcid.org/0000-0003-1757-4695

Yong Chen − *Guangzhou Institute of Energy Conversion, Chinese Academy of Sciences, Guangzhou 510640, China; CAS Key Laboratory of Renewable Energy, Guangdong Provincial Key Laboratory of New and Renewable Energy Research and Development, Guangzhou 510640, China*

Complete contact information is available at: https://pubs.acs.org/10.1021/acsomega.2c06127

Notes

The authors declare no competing financial interest.

■ ACKNOWLEDGMENTS

This research was financially supported by the State's Key Project of Research and Development Plan, China (2020YFC1908900), the National Natural Science Funds of China (51906045), the Science and Technology Program of Guangdong Province, China (2021A1515012263), the Science and Technology Program of Guangzhou, China (202002030365) and Guangdong Basic and Applied Basic Research Foundation (2021B1515020068).

■ REFERENCES

(1) Komatsuda, S.; Asakura, Y.; Vequizo, J. J. M.; Yamakata, A.; Yin, S. Enhanced photocatalytic NO decomposition of visible-light responsive F-TiO_2/(N,C)-TiO_2 by charge transfer between F-TiO_2 and (N,C)-TiO_2 through their doping levels. *Appl. Catal., B* **2018**, *238*, 358−364.

(2) Zeshan, M.; Bhatti, I. A.; Mohsin, M.; Iqbal, M.; Amjed, N.; Nisar, J.; AlMasoud, N.; Alomar, T. S. Remediation of pesticides using TiO_2 based photocatalytic strategies: A review. *Chemosphere* **2022**, *300*, No. 134525.

(3) Adeel, M.; Saeed, M.; Khan, I.; Muneer, M.; Akram, N. Synthesis and Characterization of Co−ZnO and Evaluation of Its Photocatalytic Activity for Photodegradation of Methyl Orange. *ACS Omega* **2021**, *6*, 1426−1435.

(4) Hieu, V. Q.; Phung, T. K.; Nguyen, T.-Q.; Khan, A.; Doan, V. D.; Tran, V. A.; Le, V. T. Photocatalytic degradation of methyl orange dye by Ti_3C_2−TiO_2 heterojunction under solar light. *Chemosphere* **2021**, *276*, No. 130154.

(5) Choi, H.; Shin, D.; Yeo, B. C.; Song, T.; Han, S. S.; Park, N.; Kim, S. Simultaneously controllable doping sites and the activity of a W−N codoped TiO_2 photocatalyst. *ACS Catal.* **2016**, *6*, 2745−2753.

(6) Kader, S.; Al-Mamun, M. R.; Suhan, M. B. K.; Shuchi, S. B.; Islam, M. S. Enhanced photodegradation of methyl orange dye under UV irradiation using MoO_3 and Ag doped TiO_2 photocatalysts. *Environ. Technol. Innovation* **2022**, *27*, No. 102476.

(7) Yuan, R. F.; Wang, S. N.; Liu, D.; Shao, X.; Zhou, B. H. Effect of the wavelength on the pathways of 2-MIB and geosmin photocatalytic oxidation in the presence of Fe-N co-doped TiO_2. *Chem. Eng. J.* **2018**, *353*, 319−328.

(8) Ramos, R.; Scoca, D.; Merlo, R. B.; Marques, F. C.; Alvarez, F.; Zagonel, L. F. Study of nitrogen ion doping of titanium dioxide films. *Appl. Surf. Sci.* **2018**, *443*, 619−627.

(9) Boningari, T.; Inturi, S. N. R.; Suidan, M.; Smirniotis, P. G. Novel one-step synthesis of sulfur doped-TiO_2 by flame spray pyrolysis for visible light photocatalytic degradation of acetaldehyde. *Chem. Eng. J.* **2018**, *339*, 249−258.

(10) Andoshe, D. M.; Yim, K.; Sohn, W.; Kim, C.; Kim, T. L.; Kwon, K. C.; Hong, K.; Choi, S.; Moon, C. W.; Hong, S. P.; Han, S.; Jang, H. W. One-pot synthesis of sulfur and nitrogen codoped titanium dioxide nanorod arrays for superior photoelectrochemical water oxidation. *Appl. Catal., B* **2018**, *234*, 213−222.

(11) Li, Y.; Wen, H.; Yang, J.; Zhou, Y.; Cheng, X. Boosting oxygen reduction catalysis with N, F, and S tri-doped porous graphene: Tertiary N-precursors regulates the constitution of catalytic active sites. *Carbon* **2019**, *142*, 1−12.

(12) Samokhvalov, A. Hydrogen by photocatalysis with nitrogen codoped titanium dioxide. *Renewable Sustainable Energy Rev.* **2017**, *72*, 981−1000.

(13) Andrade, O. R.; Rodriguez, V.; Camarillo, R.; Martinez, F.; Jimenez, C.; Rincon, J. Photocatalytic Reduction of CO_2 with N-Doped TiO2-Based Photocatalysts Obtained in One-Pot Supercritical Synthesis. *Nanomaterials* **2022**, *12*, No. 1793.

(14) Afzal, M. Z.; Zu, P.; Zhang, C.-M.; Guan, J.; Song, C.; Sun, X.-F.; Wang, S.-G. Sonocatalytic degradation of ciprofloxacin using hydrogel beads of TiO_2 incorporated biochar and chitosan. *J. Hazard. Mater.* **2022**, *434*, No. 128879.

(15) Chen, Y.; Wu, Q.; Zhou, C.; Jin, Q. RETRACTED: Enhanced photocatalytic activity of La and N co-doped TiO_2/diatomite composite. *Powder Technol.* **2017**, *322*, 296−300.

(16) Giannakas, A. E.; Seristatidou, E.; Deligiannakis, Y.; Konstantinou, I. Photocatalytic activity of N-doped and N-F co-doped TiO_2 and reduction of chromium(VI) in aqueous solution: An EPR study. *Appl. Catal., B* **2013**, *132*−*133*, 460−468.

(17) Zhou, F.; Song, H. B.; Wang, H. Q.; Komarneni, S.; Yan, C. J. N-doped TiO_2/sepiolite nanocomposites with enhanced visible-light catalysis: role of N precursors. *Appl. Clay Sci.* **2018**, *166*, 9−17.

(18) Kim, J. R.; Kan, E. Heterogeneous photocatalytic degradation of sulfamethoxazole in water using a biochar-supported TiO_2 photocatalyst. *J. Environ. Manage.* **2016**, *180*, 94−101.

(19) Xu, C.; Xie, W.; Si, X.; Zhang, J.; Yang, J. Photocatalytic degradation of cooking fume on a TiO_2-coated carbon nanotubes composite filter. *Environ. Res.* **2018**, *166*, 167−174.

(20) Zhang, H.; Wang, Z.; Li, R.; Guo, J.; Li, Y.; Zhu, J.; Xie, X. TiO_2 supported on reed straw biochar as an adsorptive and photocatalytic composite for the efficient degradation of sulfamethoxazole in aqueous matrices. *Chemosphere* **2017**, *185*, 351−360.

(21) Panepinto, A.; Cossement, D.; Snyders, R. Experimental and theoretical study of the synthesis of N-doped TiO2 by N ion implantation of TiO_2 thin films. *Appl. Surf. Sci.* **2021**, *541*, No. 148493.
(22) Matos, J. Eco-friendly heterogeneous photocatalysis on biochar-based materials under solar irradiation. *Top. Catal.* **2016**, *59*, 394−402.
(23) Matos, J.; Hofman, M.; Pietrzak, R. Synergy effect in the photocatalytic degradation of methylene blue on a suspended mixture of TiO_2 and N-containing carbons. *Carbon* **2013**, *54*, 460−471.
(24) Vahidzadeh, E.; Fatemi, S.; Nouralishahi, A. Synthesis of a nitrogen-doped titanium dioxide-reduced graphene oxide nanocomposite for photocatalysis under visible light irradiation. *Particuology* **2018**, *41*, 48−57.
(25) Lu, L.; Shan, R.; Shi, Y.; Wang, S.; Yuan, H. A novel TiO_2/biochar composite catalysts for photocatalytic degradation of methyl orange. *Chemosphere* **2019**, *222*, 391−398.
(26) Tang, X.; Wang, Z.; Huang, W.; Jing, Q.; Liu, N. Construction of N-doped TiO_2/MoS_2 heterojunction with synergistic effect for enhanced visible photodegradation activity. *Mater. Res. Bull.* **2018**, *105*, 126−132.
(27) Suwannaruang, T.; Kamonsuangkasem, K.; Kidkhunthod, P.; Chirawatkul, P.; Saiyasombat, C.; Chanlek, N.; Wantala, K. Influence of nitrogen content levels on structural properties and photocatalytic activities of nanorice-like N-doped TiO_2 with various calcination temperatures. *Mater. Res. Bull.* **2018**, *105*, 265−276.
(28) Dubnová, L.; Zvolská, M.; Edelmannová, M.; Matějová, L.; Martin, R.; Drobná, H.; Kuśtrowski, P.; Kočí, K.; Čapek, L. Photocatalytic decomposition of methanol-water solution over N-La/TiO_2 photocatalysts. *Appl. Surf. Sci.* **2019**, *469*, 879−886.
(29) Zeng, L.; Lu, Z.; Li, M.; Yang, J.; Song, W.; Zeng, D.; Xie, C. A modular calcination method to prepare modified N-doped TiO_2 nanoparticle with high photocatalytic activity. *Appl. Catal., B* **2016**, *183*, 308−316.
(30) Fujishima, A.; Zhang, X.; Tryk, D. TiO_2 photocatalysis and related surface phenomena. *Surf. Sci. Rep.* **2008**, *63*, 515−582.
(31) Wang, F.; Feng, L.; Zhang, D. M.; Tang, Q. G.; Feng, D. A first-principles calculation on electronic structure and optical performance of chromium and nitrogen codoped anatase titanium dioxide. *J. Alloys Compd.* **2014**, *611*, 125−129.
(32) Chen, Y. Z.; Li, A. X.; Li, Q.; Hou, X. M.; Wang, L. N.; Huang, Z. H. Facile fabrication of three-dimensional interconnected nanoporous N-TiO_2 for efficient photoelectrochemical water splitting. *J. Mater. Sci. Technol.* **2018**, *34*, 955−960.
(33) Makuła, P.; Pacia, M.; Macyk, W. How to correctly determine the band gap energy of modified semiconductor photocatalysts based on UV−vis spectra. *J. Phys. Chem. Lett.* **2018**, *9*, 6814−6817.
(34) Singh, J.; Sahu, K.; Singh, R.; Som, T.; Kotnala, R. K.; Mohapatra, S. Thermal annealing induced strong photoluminescence enhancement in Ag-TiO_2 plasmonic nanocomposite thin films. *J. Alloys Compd.* **2019**, *786*, 750−757.
(35) Sanchez-Martinez, A.; Ceballos-Sanchez, O.; Koop-Santa, C.; López-Mena, E. R.; Orozco-Guareño, E.; García-Guaderrama, M. N-doped TiO_2 nanoparticles obtained by a facile coprecipitation method at low temperature. *Ceram. Int.* **2018**, *44*, 5273−5283.
(36) Mian, M. M.; Liu, G. Recent progress in biochar-supported photocatalysts: synthesis, role of biochar, and applications. *RSC Adv.* **2018**, *8*, 14237−14248.
(37) Nguyen, C. H.; Fu, C.-C.; Juang, R.-S. Degradation of methylene blue and methyl orange by palladium-doped TiO_2 photocatalysis for water reuse: efficiency and degradation pathways. *J. Cleaner Prod.* **2018**, *202*, 413−427.
(38) Kaviyarasan, K.; Vinoth, V.; Sivasankar, T.; Asiri, A. M.; Wu, J. J.; Anandan, S. Photocatalytic and photoelectrocatalytic performance of sonochemically synthesized $Cu_2O@TiO_2$ heterojunction nanocomposites. *Ultrason. Sonochem.* **2019**, *51*, 223−229.

https://doi.org/10.1021/acsomega.2c06127
ACS Omega 2023, 8, 791−803